scientific reports

Check for updates

OPEN

Mesenchymal stem cell-derived extracellular vesicles ameliorate renal interstitial fibrosis via the miR-13474/ADAM17 axis

Linru Shi[1,2,4], Yuyan Hu[2,3,4], Houcheng Zeng[2,4], Hui Shi[2], Wenrong Xu[2], Yaoxiang Sun[1], Hong Chu[1]✉, Cheng Ji[2]✉ & Hui Qian[1,2]✉

Renal interstitial fibrosis (RIF) is a prevalent consequence of chronic renal diseases, characterized by excessive extracellular matrix (ECM) deposition. A Disintegrin and Metalloprotease 17 (ADAM17), a transmembrane metalloproteinase, plays a central role in driving renal fibrosis progression by activating Notch 1 protein and the downstream TGF-β signaling pathway. Our study investigated potential therapeutic interventions for renal fibrosis, focusing on human umbilical cord mesenchymal stem cell-derived extracellular vesicles (hucMSC-EVs). We found that hucMSC-EVs inhibit ADAM17, thereby impeding renal fibrosis progression. Analysis of hucMSC-EVs miRNA profiles revealed significant enrichment of miR-13474, which effectively targeted and inhibited ADAM17 mRNA expression, subsequently suppressing Notch1 activation, TGF-β signaling, and collagen deposition. Overexpression of miR-13474 enhanced hucMSC-EVs' inhibitory effect on renal fibrosis, while its downregulation abolished this protective effect. Our findings highlight the efficacy of hucMSC-EVs overexpressing miR-13474 in mitigating renal fibrosis via ADAM17 targeting. These insights offer potential therapeutic strategies for managing renal fibrosis.

Keywords Renal fibrosis, HucMSC, Extracellular vesicles, miR-13474, ADAM17

Chronic kidney disease (CKD) ensnares ten percent of the global populace and has risen to become the ninth leading cause of death in developed nations[1–4]. RIF emerges as the inexorable outcome of all chronic kidney diseases[5,6]. Throughout the protracted course of CKD, a fibrotic matrix is woven within the renal tissue, obliterating the organ's architectural integrity, ultimately culminating in renal failure[7,8]. Regrettably, efficacious clinical remedies for the mitigation of renal fibrosis remain elusive. Consequently, the imperative of devising an efficacious panacea for this affliction is now paramount. As CKD continues to exert its toll on global health, the urgency to develop innovative therapeutic strategies aimed at combating renal fibrosis becomes increasingly apparent.

ADAM17 epitomizes a quintessential zinc-dependent proteolytic enzyme within the ADAM family[9]. ADAM17 orchestrates complex molecular cascades that contribute to renal inflammatory and fibrotic processes[10]. Hyperexpression of ADAM17 has been found to repress ACE2 expression by modulating the TGF-β/Smad3 signaling axis, exacerbating the fibrotic phenotype[11]. Moreover, ADAM17 exerts an inhibitory influence on mitochondrial autophagy, primarily through the instigation of ER stress, further accentuating fibrotic manifestations[12]. Given the intricate involvement of ADAM17 in renal fibrosis, exploring novel therapeutic interventions targeting this protease becomes imperative. Our research found that hucMSC-EVs could down-regulate ADAM17 expression, thereby inhibiting renal fibrosis in a unilateral ureteral obstruction (UUO) model.

Recent study underscores the considerable potential of mesenchymal stem cells (MSCs) in regenerative medicine, particularly in alleviating renal fibrosis[13,14]. Despite the promise of MSC-based therapies, it's essential to acknowledge inherent limitations such as allogeneic immune rejection precocious cellular differentiation and

[1]Center for Molecular & Imageology of Jiangsu University, Division of Nephrology, The Affiliated Yixing Hospital of Jiangsu University, Yixing 214200, Jiangsu, China. [2]Jiangsu Key Laboratory of Medical Science and Laboratory Medicine, Department of Laboratory Medicine, School of Medicine, Jiangsu University, 301 Xuefu Road, Zhenjiang 212013, Jiangsu, China. [3]Shaoxing Central Hospital Medical Alliance General Hospital, The Department of Laboratory, Shaoxing 312030, Zhejiang, China. [4]These authors contributed equally: Linru Shi, Yuyan Hu and Houcheng Zeng. ✉email: staff352@yxph.com; 18252586810@163.com; 1000007341@ujs.edu.cn

malignant transformation[15]. However, recent groundbreaking discoveries suggest that the therapeutic effect of MSCs in renal fibrosis may primarily stem from the secretion of extracellular vesicles (EVs), nanoscale entities rich in lipids, nucleic acids, and proteins[16–18]. MSC-EVs present a promising, cell-free therapeutic strategy for renal diseases, addressing the limitations of MSC-based therapies[19,20]. Our previous research has demonstrated the efficacy of MSC-EVs in mitigating renal fibrosis[5]. Specifically, we found that EVs derived from hucMSC-EVs orchestrate the ubiquitination and subsequent degradation of YAP through the delivery of CK1δ and β-TRCP, thereby ameliorating renal fibrosis[5]. However, while the efficacy of MSC-EVs in targeting YAP degradation has been elucidated, their potential to modulate other factors like ADAM17 in the context of renal fibrosis remains an open question, warranting further scientific inquiry.

In our investigation, we aimed to explore the potential of MSC-EVs in mitigating renal fibrosis by targeting ADAM17. RIF often develops due to increased expression of ADAM17 in response to mechanical stress. Our results demonstrate that treatment with MSC-EVs effectively inhibits ADAM17, thus offering protection against renal fibrosis. Mechanistically, MSC-EVs carry miR-13474, which targets ADAM17 mRNA, leading to reduced expression of ADAM17 in the kidney. This targeted inhibition of ADAM17 by miR-13474 encapsulated within MSC-EVs highlights a novel therapeutic mechanism for combating renal fibrosis. In conclusion, our findings provide compelling evidence that MSC-EVs, through the miR-13474/ADAM17 axis, offer effective intervention against renal fibrosis. These insights hold significant promise for clinical therapeutic strategies.

Results

Characteristics and therapy of MSC-EVs in renal fibrosis

We isolated MSCs from human umbilical cords and subjected them to rigorous assays to characterize the derived extracellular vesicles (EVs). After isolation, MSCs were assessed for their differentiation potential using Oil Red O and Alizarin Red staining, confirming their capacity for adipogenic and osteogenic differentiation (see Supplementary Fig S1A,B online). Subsequently, MSCs were cultured in a specialized conditioned medium to yield MSC-EVs. Ultrastructural characterization of MSC-EVs was conducted using transmission electron microscopy (TEM) and nanoparticle tracking analysis (NTA). TEM images revealed a near-spherical morphology of the vesicles with an average diameter of 164 ± 62.9 nm (Fig. 1A, see Supplementary Fig. S1C online). Atomic force microscopy (AFM) further corroborated these findings, displaying MSC-EVs as typical circular structures (see Supplementary Fig. S1D online). Western blot results showed that MSC-EVs expressed EVs-associated specific proteins such as CD9, CD81, and TSG101, and negative expression of Calnexin (see Supplementary Fig. S1E online).

To assess the potential therapeutic effects of MSC-EVs on renal fibrosis, we established a comprehensive experimental model using 8-week-old SD rats subjected to UUO for 14 days. Concurrently, we initiated a 7-day treatment regimen with MSC-EVs, commencing at the onset of fibrotic induction (Fig. 1A). Utilizing DiR labeling, we tracked the biodistribution of MSC-EVs in vivo, observing a predominant accumulation of fluorescent signal within the injured renal tissue 48 h post-administration (Fig. 1B,C). Histological analyses of kidney tissue sections revealed marked alterations in renal architecture and collagen deposition, with MSC-EV treatment demonstrating mitigating effects on these fibrotic changes (Fig. 1D). Immunohistochemical staining further supported these observations, showing reduced expression of fibrosis-associated proteins (α-SMA, Collagen I) in MSC-EV-treated rats compared to UUO controls (Fig. 1D). To complement our in vivo findings, we investigated the impact of MSC-EVs on fibrosis-related gene expression in HK-2 cells using cellular fluorescence, qRT-PCR, and Western blot analyses. TGF-β treatment induced upregulation of α-SMA and Collagen I expression in HK-2 cells, indicative of a pro-fibrotic effect. In contrast, MSC-EVs attenuated the expression of these fibrosis markers, demonstrating their potential anti-fibrotic effects in vitro (Fig. 1E–H, see Supplementary Fig. S1F online). Subsequent analysis of RNA and protein extracted from renal tissues corroborated these findings, showing reduced expression of fibrosis markers in MSC-EV-treated rats compared to UUO controls (Fig. 1I, J, see Supplementary Fig. S1G online). Together, these results provide compelling evidence that MSC-EVs possess the capability to impede renal fibrosis progression, both in vivo and in vitro.

MSC-EVs alleviate renal fibrosis by inhibiting ADAM17

Numerous studies have highlighted the role of ADAM17 in activating the Notch signaling pathway, contributing to fibrogenesis[21,22]. However, the potential of MSC-EVs to inhibit ADAM17 and alleviate renal fibrosis remains underexplored. To address this gap, we conducted a series of experiments to investigate the therapeutic effects of MSC-EVs. Initially, we assessed ADAM17 protein expression in the kidneys of UUO rats using multiple techniques, including immunofluorescence, immunohistochemistry, and Western blot analysis (Fig. 2A,C,D, see Supplementary Fig. S2A online). Our results demonstrated that mechanical stress induced an upregulation of ADAM17 levels, along with increased expression of fibrosis markers such as α-SMA and collagen I. Subsequently, we administered MSC-EVs to UUO rats to examine their impact on ADAM17 expression and renal fibrosis. Remarkably, MSC-EVs exhibited a significant capacity to inhibit ADAM17 expression and attenuate the deposition of α-SMA and collagen I in the kidney (Fig. 2A,C,D, see Supplementary Fig. S2B online). To corroborate these findings, we employed TGF-β-stimulated HK-2 cells to induce fibrosis-like changes, followed by intervention with MSC-EVs. Analysis via cell fluorescence and Western blotting revealed that TGF-β stimulation led to increased ADAM17 expression, accompanied by elevated levels of fibrosis markers α-SMA and collagen I. Importantly, treatment with MSC-EVs effectively mitigated these changes (Fig. 2B,E, see Supplementary Fig. S2C online). In summary, our results indicate that MSC-EVs hold promise as a therapeutic intervention for renal fibrosis by inhibiting ADAM17 expression. These findings underscore the potential of MSC-EVs in mitigating fibrotic pathology and suggest avenues for further research in this area.

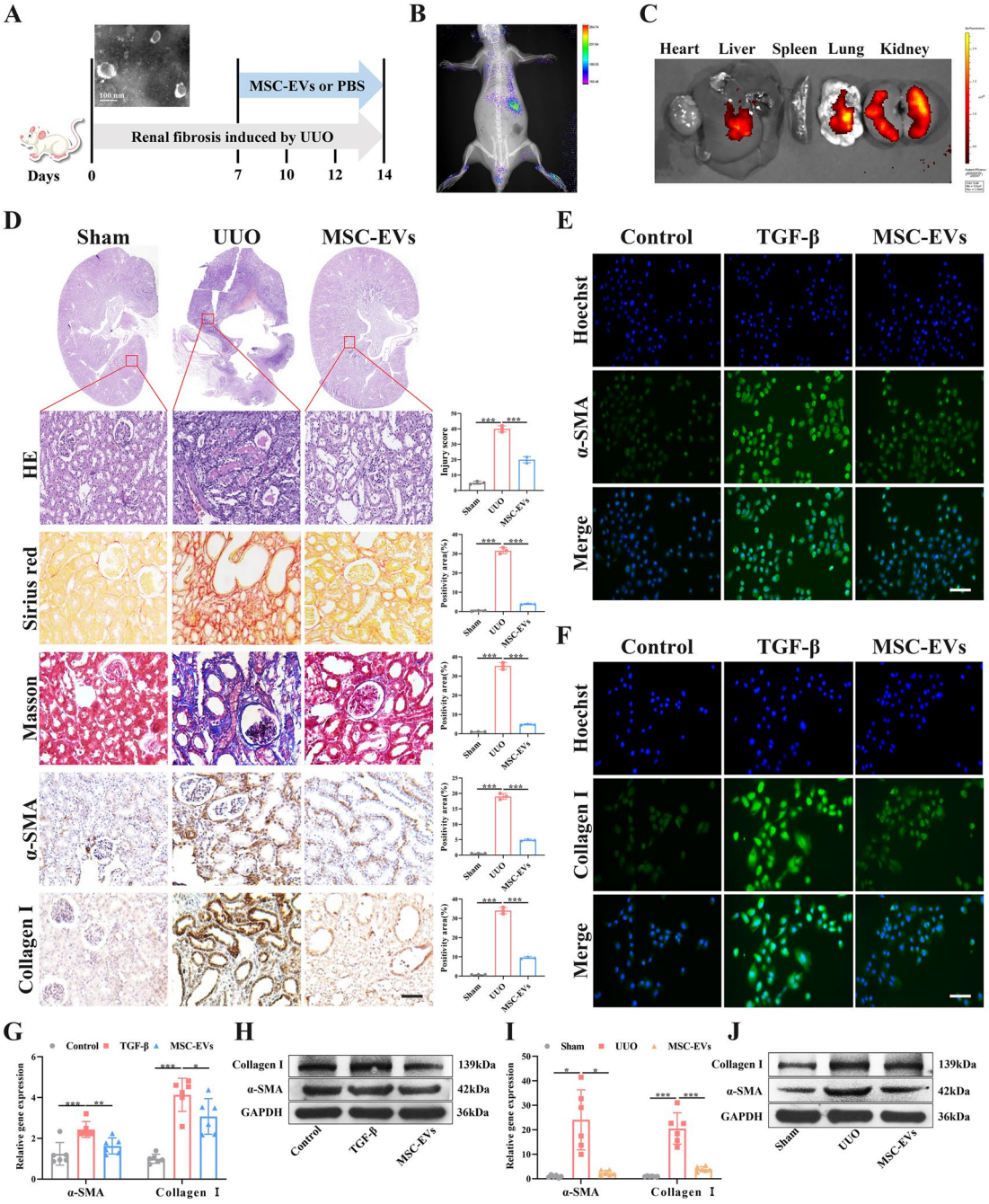

Figure 1. MSC-EVs inhibit renal fibrosis in vitro and in vivo. (**A**) TEM images of MSC-EVs and schematic diagrams of in vivo experiments. Briefly, for 14 days of UUO obstruction-induced renal fibrosis, rats were given MSC-EVs (10 mg/kg) or PBS (n = 5). Scale bar, 100 nm. (**B**) Imaging of fluorescence intensity in rats from PBS or DiR labeled MSC-EVs group at 48h post-treatment. (**C**) Fluorescence intensity imaging of heart, liver, spleen, lung and kidney of rats in PBS or DiR-labeled MSC-EVs group after 24 h of treatment. (**D**) Rat kidney tissue staining, HE staining, Sirius red staining, Masson staining, α-SMA immunohistochemical staining, Collagen I immunohistochemical staining. Scale bar, 100 μm. (**E**) Immunofluorescence staining images of α-SMA protein in HK-2 cells in the presence of TGF-β, MSC-EVs. Scale bars, 50 μm. (**F**) Immunofluorescence staining images of Collagen I protein in HK-2 cells in the presence of TGF-β, MSC-EVs. Scale bars, 50 μm. (**G**) qRT-PCR analysis of α-SMA and Collagen I mRNA in TGF-β, MSC-EVs treated HK-2 cells (n = 6). (**H**) Western blot analysis of α-SMA protein and Collagen I protein in HK-2 cells treated with TGF-β, MSC-EVs (n = 3). (**I**) qRT-PCR analysis of α-SMA and Collagen I expression in kidney tissues of UUO rats (n = 6). (**J**) Western blot detection of α-SMA protein and Collagen I protein expression in kidney tissues of UUO rats (n = 3). All data are presented as means ± SEM. *P < 0.05, **P < 0.01 and ***P < 0.001. Original blots are presented in Supplementary Fig. S7.

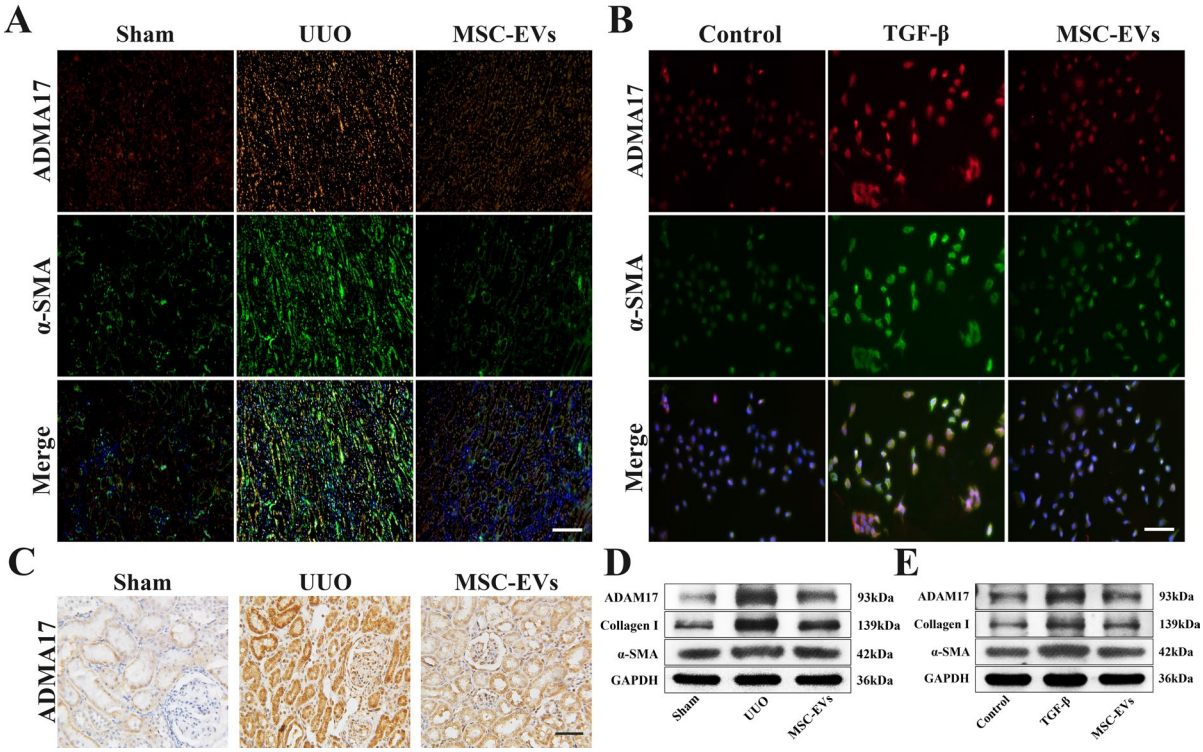

Figure 2. MSC-EVs suppress ADAM17 to mitigate renal fibrosis. (**A**) Dual immunofluorescent staining of ADAM17 (red) and α-SMA (green) in the kidneys of control rats and UUO rats. Scale bars, 100 μm. (**B**) Immunofluorescent staining images of ADAM17 (red) and α-SMA (green) proteins in HK-2 cells treated with PBS or TGF-β. Scale bars, 50 μm. (**C**) Immunohistochemical staining of ADAM17 in kidney slices from UUO rats. Scale bars, 100 μm. (**D**) Western blot analysis of ADAM17, α-SMA, and Collagen I protein expression in the kidneys of control rats and UUO rats (n = 3). (**E**) Western blot analysis of ADAM17, α-SMA, and Collagen I protein expression in control and TGF-β-stimulated HK-2 cells (n = 3). All data are presented as means ± SEM. ***P < 0.001. Original blots are presented in Supplementary Fig. S8.

miR-13474 is enriched in MSC-EVs and targets ADAM17

In our pursuit to identify the bioactive constituents within MSC-EVs responsible for inhibiting ADAM17 expression and mitigating fibrotic manifestations, we conducted a comprehensive profiling of MSC-miRNAs using miRNA-seq. This analysis revealed a significant enrichment of miRNA-13474 within MSC-EVs, comprising approximately 1% of the total repertoire (Fig. 3A). And then we plotted the structure (Fig. 3B). Subsequent comparative quantification through qRT-PCR showed a remarkable 400-fold enrichment of miR-13474 in MSC-EVs compared to HFL-EVs (extracellular vesicles derived from human embryonic lung fibroblasts) (Fig. 3C). The qRT-PCR results showed that miR-13474 was highly enriched in MSC-EVs compared to MSCs (Fig. 3D). Additionally, miR-13474 expression was found to be downregulated in the kidneys of UUO rats, which was alleviated after treatment with MSC-EVs (see Supplementary Fig. S3A online). Further investigation using Target Scan and a dual-luciferase reporter assay confirmed that miR-13474 targets the 3'UTR domain of ADAM17 (Fig. 3E). Moreover, transfection with miR-13474 mimic resulted in a significant suppression of ADAM17 protein expression, while inhibition of miR-13474 led to an increase in ADAM17 expression (see Supplementary Fig. S3B,C online). To elucidate the role of MSC-EVs-derived miR-13474 in ADAM17 modulation, we incorporated miR-13474 mimic into MSC-EVs through sonication. qRT-PCR analyses confirmed a pronounced upregulation of miR-13474 in the overexpressed MSC-EVs, denoted as miR-13474^{mimic}-MSC-EVs (Fig. 3F). Western blot findings further demonstrated that miR-13474^{mimic}-MSC-EVs significantly suppressed ADAM17 protein synthesis (Fig. 3G, see Supplementary Fig. S3D online). Interestingly, a noticeable decrease in miR-13474 expression was observed in EVs obtained from MSCs transfected with the miR-13474 inhibitor (miR-13474^{inhibitor}-MSC-EVs), particularly when compared to EVs from MSCs transfected with a negative control miRNA (miR-13474$^{inhibitor\ NC}$-MSC-EVs) (Fig. 3H). Moreover, Western blot analyses revealed that the attenuation in ADAM17 protein synthesis induced by miR-13474$^{inhibitor\ NC}$-MSC-EVs was counteracted by miR-13474^{inhibitor}-MSC-EVs (Fig. 3I, see Supplementary Fig. S3E online). These findings underscore the pivotal role of miR-13474, harbored within MSC-EVs, in orchestrating the downregulation of ADAM17 and highlight its potential therapeutic significance in mitigating renal fibrosis.

Overexpression of miR-13474 in MSC-EVs enhances inhibition of renal fibrosis

To further evaluate the therapeutic potential of miR-13474 in renal fibrosis treatment, we injected miR-13474^{mimic}-MSC-EVs and miR-13474$^{mimic\ NC}$-MSC-EVs into UUO rats. Histological analyses, including HE

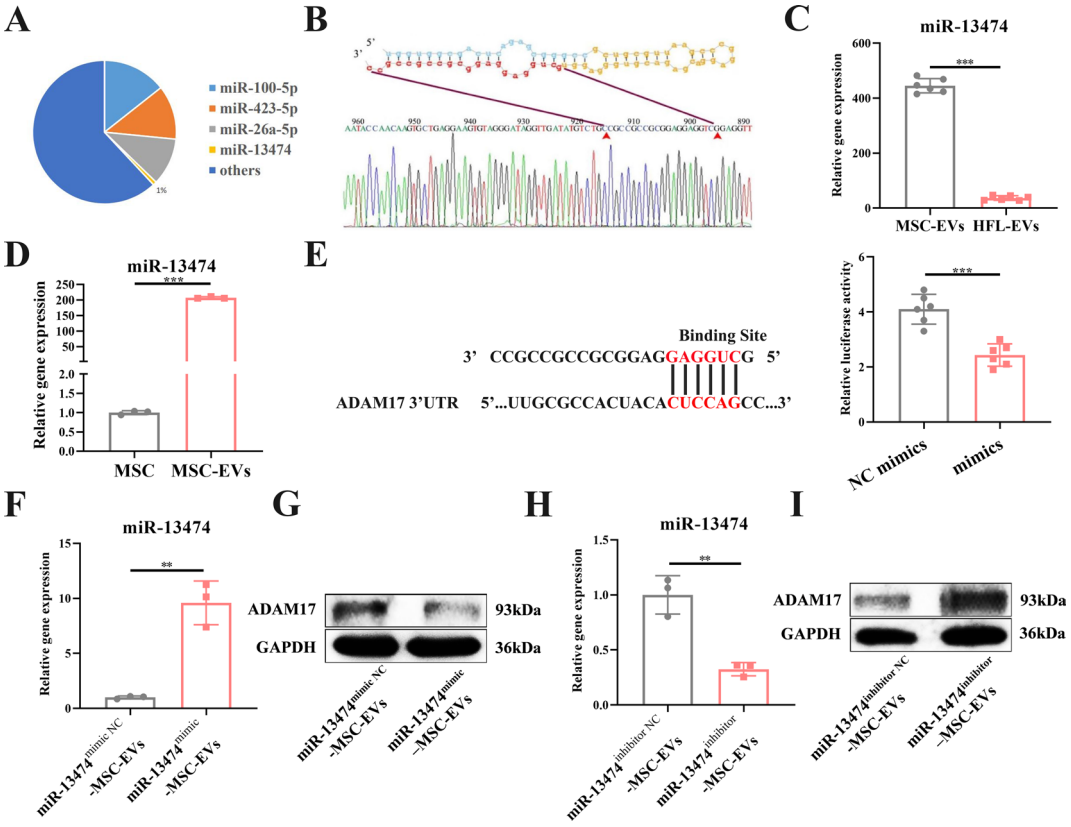

Figure 3. miR-13474 enriched in MSC-EVs and downregulated ADAM17 expression. (**A**) Relative percentage of miRNAs in total miRNA reads. (**B**) miR-13474 structure and sequencing results. (**C**) qRT-PCR to compare the expression of miR-13474 in extracellular vesicles of MSC and HFL (human embryonic lung fibroblasts) (n = 6). (**D**) qRT-PCR for miR-13474 in isolated MSCs and MSC-EVs (n = 3). (**E**) The predicted binding site of miR-13474 targeting the 3′-UTR of ADAM17; Luciferase reporter assay showed ADAM17 as a target of miR-13474 (n = 6). (**F**) qRT-PCR of miR-13474 in EVs isolated from negative control (NC) mimics overexpressed MSC-EVs (miR-13474$^{\text{mimic NC}}$-MSC-EVs) or miR-13474 mimics overexpressed MSC-EVs (miR-13474$^{\text{mimic}}$-MSC-EVs) (n = 3). (**G**) Western blot detection of ADAM17 protein expression under miR-13474$^{\text{mimic}}$-MSC-EVs treatment (n = 3). (**H**) qRT-PCR analysis of miR-13474 in EVs isolated from NC inhibitors transfected MSC (miR-13474$^{\text{inhibitor NC}}$-MSC-EVs), or miR-13474 inhibitors transfected MSC (miR-13474$^{\text{inhibitor}}$-MSC-EVs) (n = 3). (**I**) Western blot detection of ADAM17 under miR-13474$^{\text{inhibitor}}$-MSC-EVs treatment (n = 3). All data are presented as means ± SEM. **P < 0.01 and ***P < 0.001. Original blots are presented in Supplementary Fig. S9.

staining, Sirius Red, and Masson staining, revealed that miR-13474$^{\text{mimic}}$-MSC-EVs effectively preserved the structural integrity of the renal tissue and reduced collagen accumulation in the interstitial matrix, as evidenced by decreased hypertrophic manifestations in the glomerular basement membrane (Fig. 4A). Immunohistochemical examination further confirmed a significant decrease in fibrotic markers (α-SMA, Collagen I) following miR-13474$^{\text{mimic}}$-MSC-EVs administration (Fig. 4A). In co-administration experiments with HK-2 cells treated with TGF-β, miR-13474$^{\text{mimic}}$-MSC-EVs, and miR-13474$^{\text{mimic NC}}$-MSC-EVs, molecular assays including cytofluorescence, qRT-PCR, and Western blotting consistently showed reduced expression of α-SMA and Collagen I in cells treated with miR-13474$^{\text{mimic}}$-MSC-EVs (Fig. 4B–E, see Supplementary Fig. S4A online). These findings were further validated by analyzing RNA and protein expression in renal tissues, where miR-13474$^{\text{mimic}}$-MSC-EVs exhibited a significant suppression of fibrotic indicators compared to miR-13474$^{\text{mimic NC}}$-MSC-EVs (Fig. 4F,G, see Supplementary Fig. S4B online). In summary, miR-13474$^{\text{mimic}}$-MSC-EVs demonstrated robust anti-fibrotic efficacy both in vivo and in vitro, highlighting their potential as a therapeutic intervention for renal fibrosis.

Knockdown of miR-13474 in MSC-EVs attenuates efficacy in inhibiting renal fibrosis

To further explicate the modulatory role of miR-13474 in tempering fibrogenic advancement, we instigated interventional strategies in SD rats subjected to UUO. These involved the administration of miR-13474$^{\text{inhibitor}}$-MSC-EVs, in conjunction with an isogenic cohort administered vesicles containing a negative inhibitor (classified as miR-13474$^{\text{inhibitor NC}}$-MSC-EVs). HE staining corroborated a salient exacerbation in renal structural degradation and a conspicuous augmentation in glomerular basement membrane thickness in the miR-13474$^{\text{inhibitor}}$-MSC-EVs treated rats compared to miR-13474$^{\text{inhibitor NC}}$-MSC-EVs (Fig. 5A). Sirius Red and Masson staining, unambiguously delineated a palpable accretion of collagenous fibrils within the renal interstitial space of the miR-13474$^{\text{inhibitor}}$-MSC-EVs experimental cadre relative to the miR-13474$^{\text{inhibitor NC}}$-MSC-EVs group (Fig. 5A).

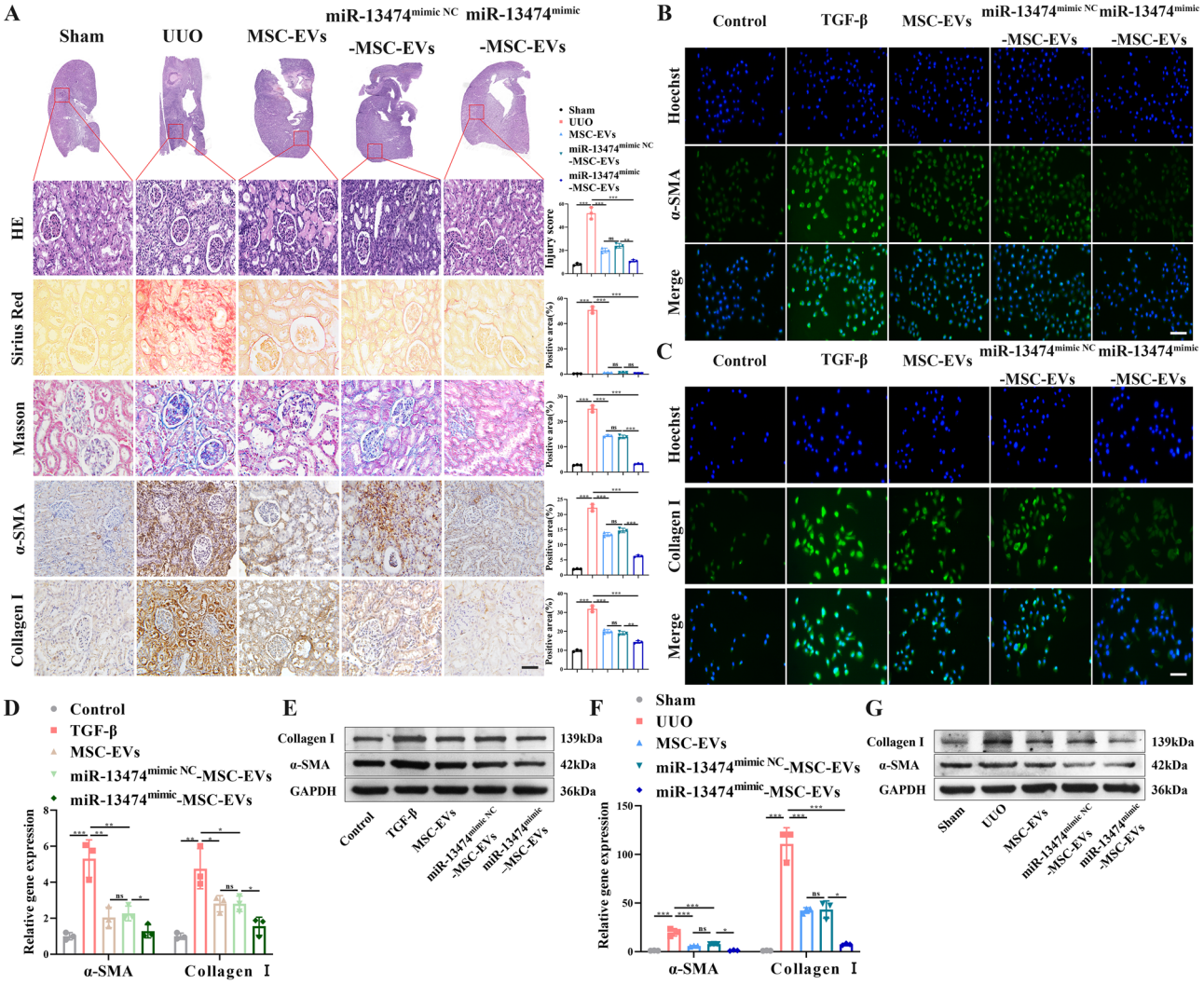

Figure 4. miR-13474 overexpression enhances the inhibitory effect of MSC-EVs on fibrosis. (**A**) Kidney tissue staining, HE staining, Sirius red staining, Masson staining, α-SMA immunohistochemical staining, Collagen I immunohistochemical staining in UUO rats after miR-13474$^{\text{mimic NC}}$-MSC-EVs and miR-13474$^{\text{mimic}}$-MSC-EVs treatment. Scale bar, 100 μm. (**B**) Immunofluorescence staining images of α-SMA protein in HK-2 cells in the presence of TGF-β, miR-13474$^{\text{mimic NC}}$-MSC-EVs and miR-13474$^{\text{mimic}}$-MSC-EVs. Scale bars, 50 μm. (**C**) Immunofluorescence staining images of Collagen I protein in HK-2 cells in the presence of TGF-β, miR-13474$^{\text{mimic NC}}$-MSC-EVs and miR-13474$^{\text{mimic}}$-MSC-EVs. Scale bars, 50 μm. (**D**) qRT-PCR analysis of α-SMA and Collagen I mRNA in HK-2 cells treated with TGF-β, miR-13474$^{\text{mimic NC}}$-MSC-EVs and miR-13474$^{\text{mimic}}$-MSC-EVs (n = 3). (**E**) Western blot analysis of α-SMA protein and Collagen I protein in TGF-β, miR-13474$^{\text{mimic NC}}$-MSC-EVs and miR-13474$^{\text{mimic}}$-MSC-EVs treated HK-2 cells (n = 3). (**F**) qRT-PCR analysis of α-SMA and Collagen I expression in kidney tissues of miR-13474$^{\text{mimic NC}}$-MSC-EVs and miR-13474$^{\text{mimic}}$-MSC-EVs treated UUO rats (n = 3). (**G**) Western blot detection of α-SMA protein and Collagen I protein expression in renal tissues of UUO rats after treatment with miR-13474$^{\text{mimic NC}}$-MSC-EVs and miR-13474$^{\text{mimic}}$-MSC-EVs (n = 3). All data are presented as means ± SEM. ns, not significant, *P < 0.05, **P < 0.01 and ***P < 0.001. Original blots are presented in Supplementary Fig. S10.

Immunohistochemical scrutinies, specifically targeting quintessential fibrogenic markers α-SMA and Collagen I, manifested an augmented expression within the miR-13474$^{\text{inhibitor}}$-MSC-EVs cohort (Fig. 5A). This was further substantiated through an array of multifaceted molecular techniques, encompassing cytofluorescence (Fig. 5B,C), qRT-PCR (Fig. 5D), and Western blot analyses (Fig. 5E, see Supplementary Fig. S5A online), which consistently attested to an upregulation of α-SMA and Collagen I transcripts and proteins in the presence of miR-13474$^{\text{inhibitor}}$-MSC-EVs. Through the exhaustive isolation and molecular scrutiny of RNA and protein constituents from renal tissue specimens, our findings, corroborated by both qRT-PCR (Fig. 5F) and Western blot (Fig. 5G, see Supplementary Fig. S5B online), distinctly affirm that miR-13474$^{\text{inhibitor}}$-MSC-EVs elicited a pronounced upregulation of salient fibrotic biomarkers—specifically α-SMA and Collagen I—in contradistinction to the miR-13474$^{\text{inhibitor NC}}$-MSC-EVs. These cogent findings robustly advocate for the influential role of MSC-EVs in the targeted inhibition of fibrotic development, mediated through the regulatory action of miR-13474.

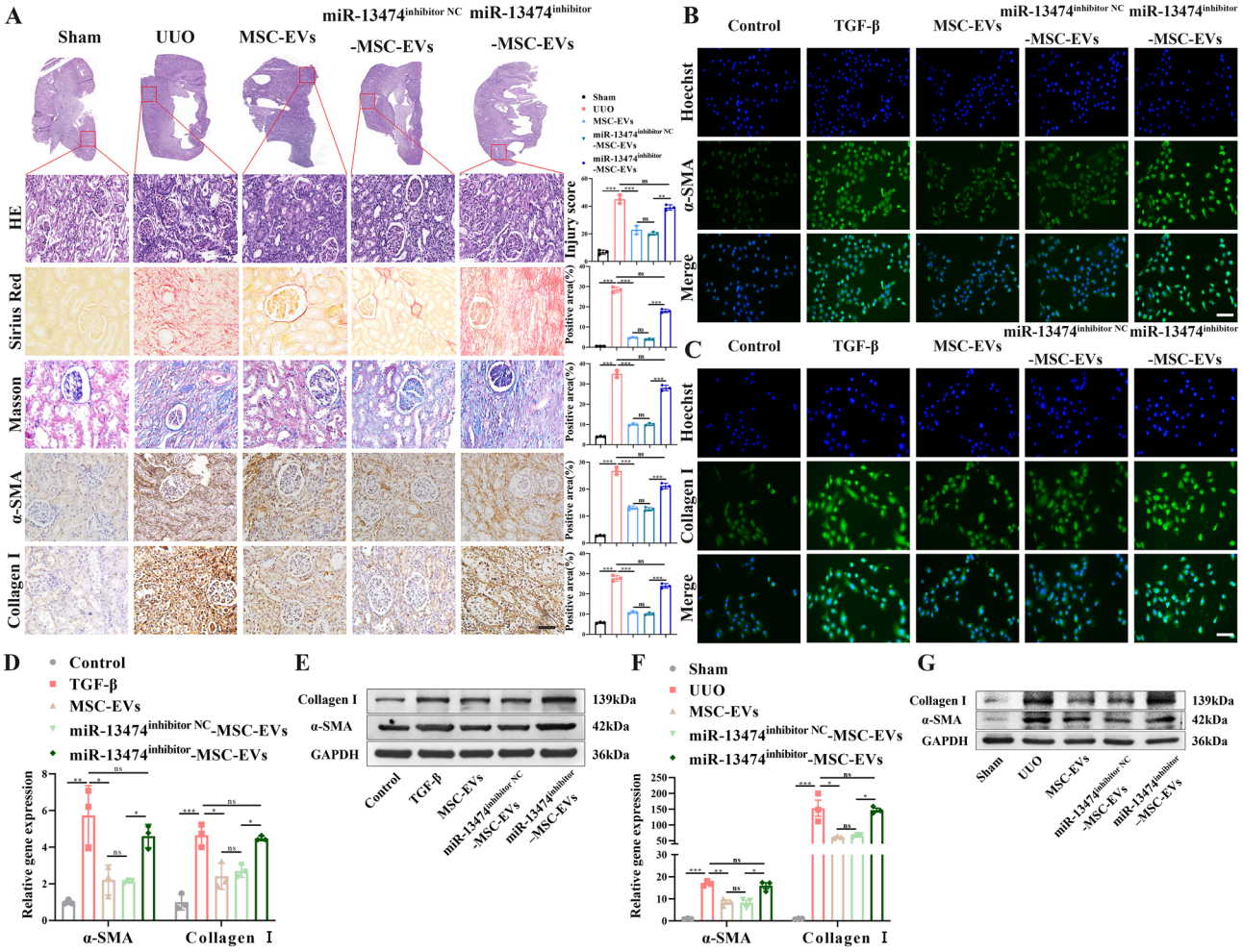

Figure 5. miR-13474 knockdown attenuates the inhibitory effect of MSC-EVs on fibrosis. (**A**) Kidney tissue staining, HE staining, Sirius red staining, Masson staining, α-SMA immunohistochemical staining, Collagen I immunohistochemical staining in UUO rats after miR-13474$^{\text{inhibitor NC}}$-MSC-EVs and miR-13474$^{\text{inhibitor}}$-MSC-EVs treatment. Scale bar, 100 μm. (**B**) Immunofluorescence staining images of α-SMA protein in HK-2 cells in the presence of TGF-β, miR-13474$^{\text{inhibitor NC}}$-MSC-EVs and miR-13474$^{\text{inhibitor}}$-MSC-EVs. Scale bars, 50 μm. (**C**) Immunofluorescence staining images of Collagen I protein in HK-2 cells in the presence of TGF-β, miR-13474$^{\text{inhibitor NC}}$-MSC-EVs and miR-13474$^{\text{inhibitor}}$-MSC-EVs. Scale bars, 50 μm. (**D**) qRT-PCR analysis of α-SMA and Collagen I mRNA in HK-2 cells treated with TGF-β, miR-13474$^{\text{inhibitor NC}}$-MSC-EVs and miR-13474$^{\text{inhibitor}}$-MSC-EVs (n = 3). (**E**) Western blot analysis of α-SMA protein and Collagen I protein in TGF-β, miR-13474$^{\text{inhibitor NC}}$-MSC-EVs and miR-13474$^{\text{inhibitor}}$-MSC-EVs treated HK-2 cells (n = 3). (**F**) qRT-PCR analysis of α-SMA and Collagen I expression in kidney tissues of UUO rats after miR-13474$^{\text{inhibitor NC}}$-MSC-EVs and miR-13474$^{\text{inhibitor}}$-MSC-EVs treatment (n = 3). (**G**) Western blot was used to detect the expression of α-SMA protein and Collagen I protein in kidney tissues of UUO rats after miR-13474$^{\text{inhibitor NC}}$-MSC-EVs and miR-13474$^{\text{inhibitor}}$-MSC-EVs treatment (n = 3). All data are presented as means ± SEM. ns, not significant, *P < 0.05, **P < 0.01 and ***P < 0.001. Original blots are presented in Supplementary Fig. S11.

miR-13474 in MSC-EVs attenuates renal fibrosis via ADAM17 downregulation

In order to verify that miR-13474 in MSC-EVs alleviated renal fibrosis by inhibiting ADAM17, we performed the following series of experiments. Immunohistochemical assessments elegantly delineated that miR-13474$^{\text{mimic}}$-MSC-EVs precipitated a noteworthy diminution in ADAM17 expression compared to miR-13474$^{\text{mimic NC}}$-MSC-EVs, whereas in juxtaposition, the presence of miR-13474$^{\text{inhibitor}}$-MSC-EVs conspicuously amplified ADAM17 expression compared to miR-13474$^{\text{inhibitor NC}}$-MSC-EVs (Fig. 6A, see Supplementary Fig. S6A online). Employing cytofluorescence (Fig. 6B), qRT-PCR (Fig. 6C), and western blot (Fig. 6E), we ascertained that TGF-β exerted a pronounced influence by enhancing ADAM17 expression and elevating the levels of fibrosis-related markers, while concurrently down-regulating the expression of Notch 1. Overexpression of miR-13474 had the opposite effect, whereas the presence of miR-13474 inhibitor significantly increased the expression of ADAM17 and related fibrosis markers while downregulating Notch 1 expression (Fig. 6B,C,E, see Supplementary Fig. S6B online). Subsequent to rigorous extraction and molecular scrutiny of RNA and proteinaceous constituents from renal tissues, our initial inferences were strongly supported (Fig. 6D,F, see Supplementary Fig. S6C online). We transfected

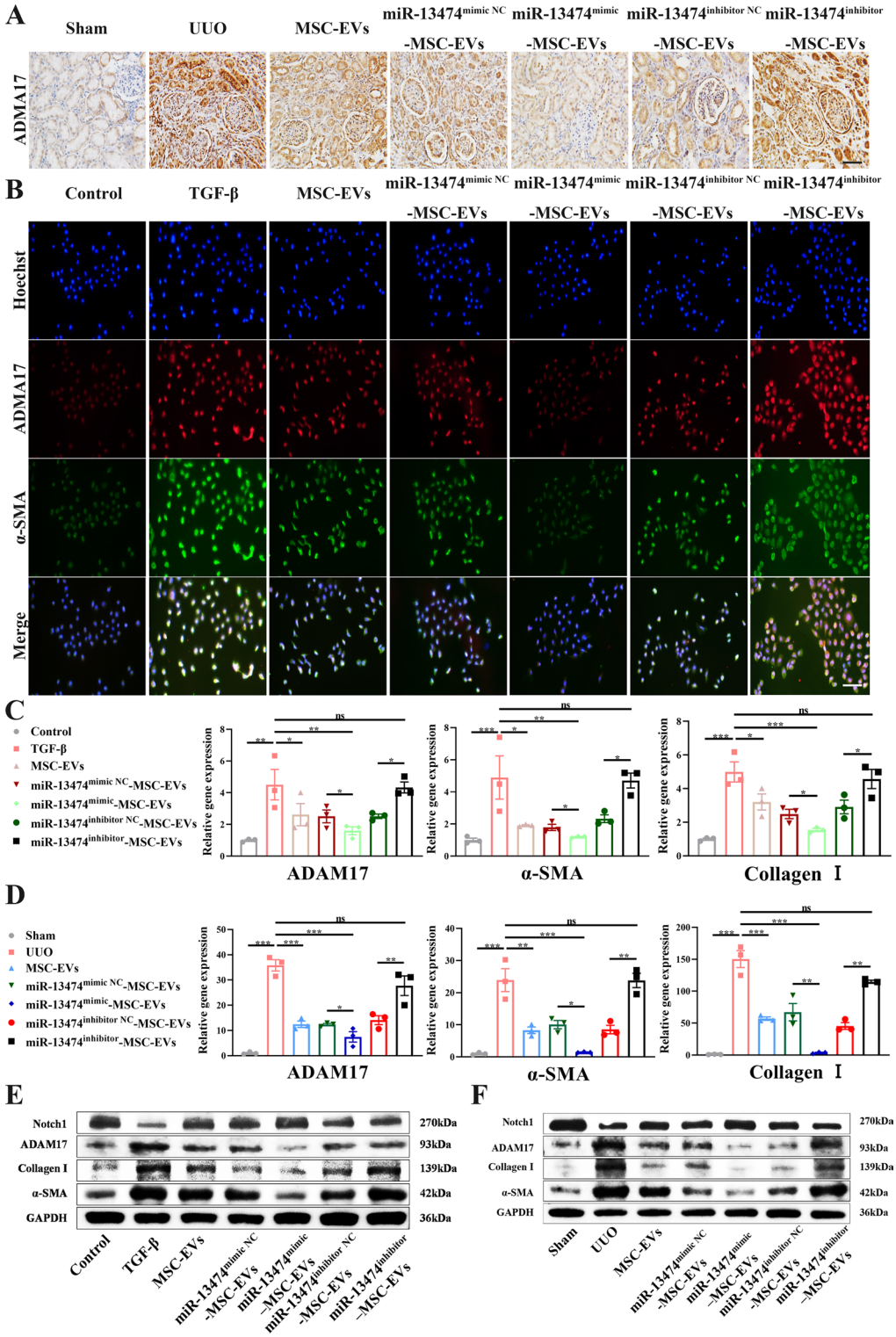

Figure 6. miR-13474 targets ADAM17 to inhibit fibrosis. (**A**) Immunohistochemical staining for ADAM17 in kidney tissues of UUO rats after miR-13474$^{\text{mimic NC}}$-MSC-EVs, miR-13474$^{\text{mimic}}$-MSC-EVs, miR-13474$^{\text{inhibitor NC}}$-MSC-EVs and miR-13474$^{\text{inhibitor}}$ treatment. Scale bar, 100 μm. (**B**) Images of immunofluorescence staining for ADAM17 (red) and α-SMA (green) in HK-2 cells treated with miR-13474$^{\text{mimic NC}}$-MSC-EVs, miR-13474$^{\text{mimic}}$-MSC-EVs, miR-13474$^{\text{inhibitor NC}}$-MSC-EVs and miR-13474$^{\text{inhibitor}}$. Scale bars, 50 μm. (**C**) qRT-PCR for ADAM17, α-SMA and Collagen I mRNA in miR-13474$^{\text{mimic NC}}$-MSC-EVs, miR-13474$^{\text{mimic}}$-MSC-EVs, miR-13474$^{\text{inhibitor NC}}$-MSC-EVs and miR-13474$^{\text{inhibitor}}$-MSC-EVs treated HK-2 cells (n = 3). (**D**) qRT-PCR detection of ADAM17, α-SMA and Collagen I mRNA expression in kidney tissues of miR-13474$^{\text{mimic NC}}$-MSC-EVs, miR-13474$^{\text{mimic}}$-MSC-EVs, miR-13474$^{\text{inhibitor NC}}$-MSC-EVs and miR-13474$^{\text{inhibitor}}$-MSC-EVs treated UUO rats (n = 3). (**E**) Western blot analysis of Notch 1, ADAM17, α-SMA and Collagen I proteins in miR-13474$^{\text{mimic NC}}$-MSC-EVs, miR-13474$^{\text{mimic}}$-MSC-EVs, miR-13474$^{\text{inhibitor NC}}$-MSC-EVs and miR-13474$^{\text{inhibitor}}$-MSC-EVs treated HK-2 cells (n = 3). (**F**) Western blot analysis of Notch 1, ADAM17, α-SMA and Collagen I protein expression in kidney tissues of miR-13474$^{\text{mimic NC}}$-MSC-EVs, miR-13474$^{\text{mimic}}$-MSC-EVs, miR-13474$^{\text{inhibitor NC}}$-MSC-EVs and miR-13474$^{\text{inhibitor}}$-MSC-EVs treated UUO rats (n = 3). All data are presented as means ± SEM. ns, not significant, *P < 0.05, **P < 0.01 and ***P < 0.001. Original blots are presented in Supplementary Fig. S12.

ADAM17 siRNA into HK-2 cells and observed a reduction in the levels of ADAM17 and fibrotic markers (α-SMA, Collagen I) through Western blot analysis (see Supplementary Fig. S6D online). Collectively, this corpus of empirical data provides incontrovertible evidence for the instrumental role of miR-13474, contained within extracellular vesicles, in ameliorating fibrotic pathogenesis via the intricate modulation of ADAM17.

Discussion

Renal fibrosis represents a progressive deterioration, characterized by an imbalance between protein synthesis and catabolism within the ECM, ultimately leading to the accumulation of fibrotic scar tissue, primarily composed of collagen I[23]. ADAM17 has emerged as a pivotal player in this pathological process, modulating ECM deposition and collagen crosslinking by influencing AMPK signaling through ADRA1A[24]. Building upon this understanding, our study sought to investigate the therapeutic potential of MSC-EVs in alleviating renal fibrosis. Specifically, we focused on elucidating the mechanism by which MSC-EVs target ADAM17 expression in a rat model of UUO-induced renal fibrosis. Our findings revealed that MSC-EVs are enriched with miR-13474, a microRNA implicated in the regulation of ADAM17 expression. Through the orchestrated release of miR-13474, MSC-EVs effectively downregulate ADAM17 expression, thereby attenuating renal fibrosis. These insights provide a novel and clinically viable strategy for targeting ADAM17 and mitigating renal fibrosis using MSC-EVs.

ADAM17 plays a crucial role in renal fibrosis by amplifying the expression of EGFR ligand dual regulatory protein (pro-AREG), which activates EGFR and promotes the release of pro-fibrotic factors, exacerbating renal fibrosis[25]. Additionally, ADAM17 cleaves the Notch1 receptor, releasing the Notch intracellular domain (NICD1), which translocates to the nucleus and induces the expression of the TGF-βR1 gene[26]. This leads to the activation of TGF-β signaling and the subsequent expression of collagen I, contributing to renal fibrosis[26]. Therefore, inhibition of ADAM17 expression emerges as a promising strategy for alleviating renal fibrosis. Building upon this understanding, our study investigated the potential of DiR-labeled MSC-EVs to selectively target impaired kidneys and attenuate ADAM17 expression. Our findings provide groundbreaking evidence supporting the efficacy of MSC-EVs in inhibiting ADAM17, introducing a novel approach to mitigate renal fibrosis.

Human umbilical cord-derived MSCs offer high yield, proliferation, accessibility, and ethical acceptability[27,28]. Therefore, umbilical cord tissue emerges as a particularly advantageous reservoir for MSC isolation. In recent biomedical research, extracellular vesicles derived from MSCs are gaining recognition for their crucial role in ameliorating renal pathologies[29]. Studies have demonstrated the therapeutic potential of MSC-EVs in various renal conditions. For instance, miR-125b-5p abundantly present in MSC-EVs has been shown to rescue G2/M cell cycle arrest by repressing p53 expression in renal tubular epithelial cells, leading to the mitigation of acute kidney injury and enhancement of tubular restitution[30]. Similarly, the microRNA tandem of miR-294/miR-133, found in MSC-EVs, attenuates renal fibrosis by inhibiting TGF-β-mediated phosphorylation of SMAD2/3 and ERK1/2[31]. In our study, we employed hucMSC-EVs, administering them intravenously into rat kidneys subjected to UUO. Our experimental outcomes unequivocally demonstrate the potent capacity of hucMSC-EVs to proficiently thwart the progression of renal fibrosis. Additionally, we sequenced the miRNA expression profiles of MSC-EVs to elucidate the underlying mechanistic pathways, thereby amplifying our understanding of their therapeutic potential.

MicroRNAs (miRNAs) are non-coding, single-stranded RNA molecules approximately 22 nucleotides in length, encoded by endogenous genes, and play crucial roles in gene regulation by binding incompletely and complementarily to target genes, thus blocking translation[32]. An increasing body of research has demonstrated the therapeutic potential of miRNAs encapsulated within extracellular vesicles (EVs) in ameliorating various renal pathologies. For instance, miR-21a-5p found within bone marrow-derived MSC (BMSC)-EVs has been shown to mitigate renal fibrosis by targeting PFKM, thereby attenuating glycolytic activity[33]. Similarly, miR-374a-5p encapsulated in MSC-EVs impedes the progression of renal fibrosis via the MAPK6/MK5/YAP signaling cascade[32]. Informed by these precedents, we postulated that certain miRNAs housed within MSC-EVs could assume a vital role in diminishing renal fibrosis. To validate this hypothesis, our sequencing analysis revealed a discernable enrichment of miR-13474 within MSC-EVs. Subsequent empirical analyses demonstrated that the down-regulation of miR-13474 exacerbates renal fibrosis, while its overexpression attenuates renal fibrosis, thus substantiating its crucial role in renal fibrosis alleviation. Mechanistically, miR-13474 interacts with the 3′ Untranslated Region (3′UTR) of ADAM17, inhibiting its expression and contributing to the mitigation of renal fibrosis.

We still have a lot of work to do in the future. Firstly, further mechanistic elucidation is warranted to delve into the molecular intricacies underlying the interaction between miR-13474, ADAM17, and renal fibrosis, including the exploration of additional downstream pathways and potential crosstalk with other signaling cascades. Secondly, optimization of therapeutic approaches is essential, including determining the optimal dosage, timing, and route of administration of hucMSC-EVs to maximize their efficacy in mitigating renal fibrosis. Thirdly, translation of in vitro findings to in vivo models is crucial to validate the therapeutic potential of hucMSC-EVs overexpressing miR-13474, assessing their safety, biodistribution, and long-term effects in preclinical settings. Furthermore, clinical trials are warranted to evaluate the efficacy and safety of these EVs in patients with renal fibrosis, assessing their therapeutic benefits, potential side effects, and long-term outcomes. Finally, exploration of combination therapies involving hucMSC-EVs overexpressing miR-13474 and other therapeutic agents or modalities could provide insights into synergistic effects and potential additive benefits in mitigating renal fibrosis. These future research directions have the potential to significantly advance our understanding of renal fibrosis pathogenesis and contribute to the development of novel therapeutic strategies for clinical intervention.

In summary, the administration of MSC-EVs resulted in a significant reduction in ADAM17 expression, accompanied by a substantial decrease in collagen accumulation and the progression of renal fibrosis. Through a series of in vivo and in vitro experiments, we uncovered that MSC-EVs exert their effects by targeting and

inhibiting ADAM17, primarily through the action of miR-13474. Our experiments revealed that MSC-EVs containing miR-13474 effectively downregulate ADAM17 expression, thereby mitigating the development of renal fibrosis (Fig. 7). This mechanism underscores the therapeutic potential of MSC-EVs in combating fibrotic kidney diseases and provides valuable insights into the intricate molecular pathways involved.

Abundant in MSC-EVs, miR-13474 has demonstrated its efficacy in inhibiting ADAM17-induced collagen deposition, thus offering protective benefits to the renal environment. This protective mechanism operates through the precise targeting of ADAM17 mRNA by miR-13474. By binding to the mRNA molecule, miR-13474 impedes its translation process, ultimately leading to a reduction in ADAM17 expression.

Materials and methods

Cell culture

MSCs were isolated from umbilical cord specimens obtained with informed consent from mothers at the Affiliated Hospital of Jiangsu University. The MSCs were cultured in α-MEM (Meilunbio, China) supplemented with 10% FBS (Bovogen, Australia). Concurrently, human renal tubular epithelial cells (HK-2 cells) were cultured in DMEM (Meilunbio, China) with 10% FBS (Bovogen, Australia). Both cell types were maintained at 37 °C in a 5% CO_2 atmosphere.

Isolation and characterization of MSC-EVs

In the current experimental methodology, we isolated mesenchymal stem cell-derived supernatant to obtain extracellular vesicles. The supernatant underwent an initial low-speed centrifugation at 4 °C for 30 min at a force of 2000*g* to remove cellular detritus. Subsequently, we subjected the clarified supernatant to a higher gravitational force of 10,000*g* for an additional 30 min to eliminate residual organelles. Following this, the resulting supernatant was concentrated using an ultrafiltration tube with a molecular weight cutoff of 100 kDa and centrifuged again at 2000*g* for 30 min. Further ultracentrifugation was then performed at 4 °C and 100,000*g* for three hours, after which the supernatant was discarded, and the pellet containing MSC-EVs was reconstituted in phosphate-buffered saline. This resuspension process was repeated twice to ensure sample purity. Subsequently, the processed sample underwent filtration through a 0.22 μm pore-size membrane within a sterile laminar flow cabinet to remove bacterial contaminants. Following isolation, morphological characterization of the isolated MSC-EVs was conducted using transmission electron microscopy. The protein concentration of the extracted exosomes was quantified by a BCA protein assay kit (Pierce, ThermoFisher). Additionally, their dimensional attributes and particle concentrations were determined through Nanosight tracking analysis (NTA). These characterization

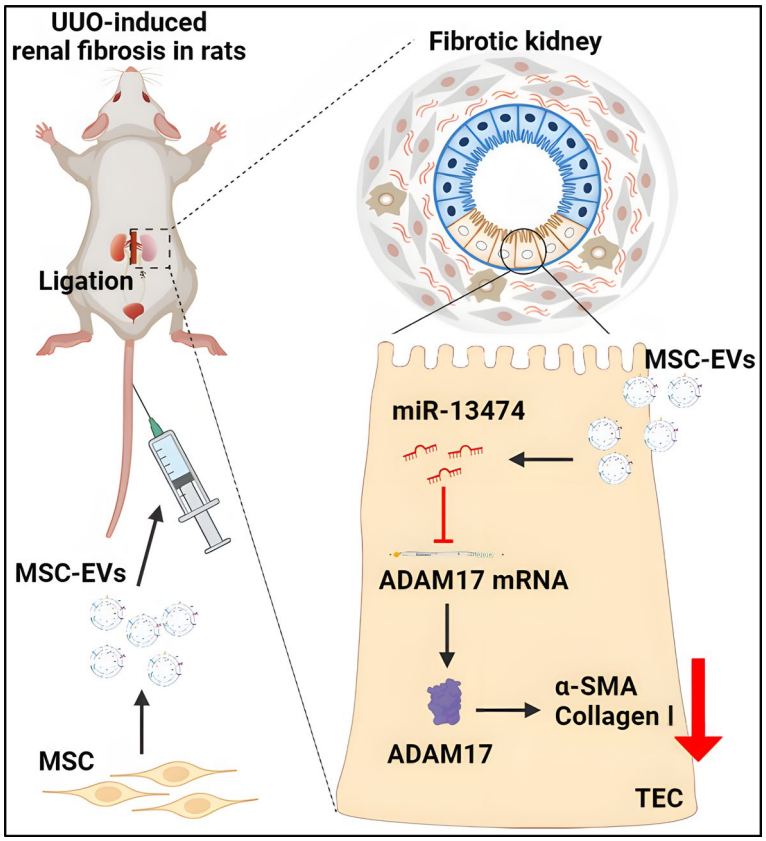

Figure 7. A proposed model for the therapeutic role of MSC-EVs in renal fibrosis.

methods provided crucial insights into the size, shape, and concentration of the MSC-EVs, aiding in further experimental analyses.

UUO rat model and MSC-EVs injection

The study was approved by the Ethics Committee for Experimental Animals of Jiangsu University (Approval number: 2020280). All participants provided written informed consent prior to research participation. All experiments were performed in accordance with relevant named guidelines and regulations. All authors complied with the ARRIVE guidelines. Female SD rats, aged eight weeks, were subjected to ureteropelvic junction ligation employing a 4.0 caliber suture via a left flank incision, under comprehensive general anesthesia, to instigate renal fibrosis. Subsequently, the murine subjects were arbitrarily allocated into seven distinct experimental cohorts: a Sham-operated control assemblage (n = 5), UUO set (n = 5), an MSC-EV administration faction at a dosage of 10 mg/kg (n = 5), an analogous assemblage receiving miR-13474$^{\text{mimic NC}}$-MSC-EVs at the same dosage (n = 5), a cohort administered with miR-13474$^{\text{mimic}}$-MSC-EVs at 10 mg/kg (n = 5), an assemblage given miR-13474$^{\text{inhibitor NC}}$-MSC-EVs at the aforementioned dosage (n = 5), and a final group receiving miR-13474$^{\text{inhibitor}}$-MSC-EVs also at 10 mg/kg (n = 5). Therapeutic agents were administered through caudal venous injections on post-operative days 7, 10, and 12. The rats were euthanized on the 14th day post-surgery, and renal tissue specimens were collected for further analysis.

Western blot

Tissue and intracellular proteins were extracted employing RIPA (Beyotime, Shanghai, China) lysis buffer. Following extraction, the quantification of these proteins was performed via the BCA (Vazyme Biotech, Nanjing, China) assay to determine their concentrations. Equal amounts of lysates were loaded and separated on a 10% or 12% SDS-PAGE gel. Subsequently, the proteins were electrotransferred onto PVDF membranes for immunoblotting. These membranes were subsequently blocked with 5% non-fat milk for a two-hour duration and incubated overnight at 4 °C with specific primary antibodies targeting relevant molecular markers. The primary antibodies employed in this rigorous analytical procedure included CD9 (1:500, Bioworld, USA, BS3022), Calnexin (1:2000, Sigma-Aldrich, USA, BS1438), TSG101 (1:1000, Abcam, UK, BS91381), α-SMA (1:500, BioWorld, USA, P62736), Collagen I (1:500, BioWorld, USA, BS70155), ADAM17 (1:500, Affinity, USA, AF6361), and GAPDH (1:2000, Abclonal, China, AC027). The analysis of these markers was performed using an ECL (Amersham Pharmacia Biotech, Little Chalfont, UK) detection system. All the original raw blots are included in the Supplementary Figs. S7–S14.

MiRNA sequencing

To investigate the differential expression of miRNAs in MSC-EVs and HFL-EVs (extracellular vesicles derived from human embryonic lung fibroblasts), miRNA sequencing was performed by OE Biotech (Shanghai, China). MSC-sEV and HFL-EVs were purified from 200 mL of cell supernatant, respectively. Following purification, total RNA was extracted from each sample. A total of 5 μg of RNA was then used for sequencing. Both ends of the RNA were ligated to adaptors, reverse transcribed into cDNA, and sequenced using an Illumina HiSeq sequencer. The sequencing data were analyzed to identify differentially expressed miRNAs, with a significance threshold set at p-value < 0.05. We then focused on miRNAs predicted to target ADAM17. Among these, miR-13474 was found to be highly expressed in MSC-EVs and was predicted to interact with ADAM17 mRNA. Compared to HFL-EVs, MSC-EVs contained significantly higher levels of miR-13474.

Quantitative reverse transcription PCR

Total RNA was isolated from cellular and tissue samples following the protocols outlined by the Trizol reagent kit (Invitrogen). After isolation, RNA concentration was precisely quantified to ensure optimal conditions for downstream analyses. The extracted RNA was then reverse transcribed into cDNA using a specialized reverse transcription kit (HiScript III 1st Strand cDNA Synthesis Kit (+ gDNA)). This step enables the conversion of RNA into a form suitable for quantitative analysis of gene expression. For quantitative analysis of target gene expression, AceQ qPCR SYBR Green Master Mix was utilized, and quantification was performed via the 2^-ΔΔCt methodology. β-Actin was employed as the endogenous reference control to normalize gene expression levels. Relevant oligonucleotide primers, synthesized by Sangon Biotech, are provided in the Supplementary Table for reference, ensuring reproducibility and accuracy in the experimental process.

Histology and immunohistochemistry

To prepare the renal tissue specimens for analysis, fixation was performed using a 4% paraformaldehyde solution. Following fixation, the specimens were carefully embedded in paraffin matrices to ensure structural integrity. Subsequently, the embedded tissue underwent a series of staining procedures to enable detailed histological examination. This included staining with Hematoxylin and Eosin (HE), Sirus red stains, and Masson stains, each serving a specific purpose in visualizing different tissue components and structures. In addition to the staining procedures, immunohistochemical assays were conducted using specific antibodies targeted against key markers. These included α-SMA (1:100, BioWorld, USA, P62736), ADAM17 (1:100, Affinity, USA, AF6361), and collagen I (1:500, BioWorld, USA, BS70155), allowing for the visualization and quantification of relevant proteins within the renal tissue. To evaluate tubular injury score, 3 random tissue sections per mouse were assessed on H&E staining and semiquantitatively scored as follows: 0, no damage; 1–5, < 25%; 6–10, 25 to ~ 50%; 11–15, 50 to ~ 75%; 16–20, > 75%. Positive areas for Sirius red, Masson, and IHC staining were semiquantified using Image Pro-Plus software (Media Cybernetics, Rockville, MD, USA).

Immunofluorescence

HK-2 cells underwent a fixation protocol with a 4% paraformaldehyde solution for a duration of 15 min, followed by permeabilization of the cellular membranes via a 0.2% Triton X-100 solution for an additional 10 min at ambient temperature. Blocking procedures were then instituted with a 5% BSA solution for a half-hour. Subsequently, the cells were subjected to overnight incubation at a temperature of 4 °C with primary antibodies specifically targeting α-SMA, anti-Collagen I, and anti-ADAM17. Post-primary antibody exposure, the cells were incubated with fluorophore-conjugated secondary antibodies for 30 min at room temperature. This was followed by nuclear counterstaining using DAPI for a period of 10 min, also conducted at ambient temperature.

Dual luciferase reporter gene assay

The putative interaction between miR-13474 and the ADAM17 gene was computationally identified via TargetScan (http://targetscan.org/) and subsequently empirically validated through dual-luciferase reporter assays. Three distinct untranslated regions (UTRs) corresponding to the human ADAM17 gene, each encompassing either the wild-type (WT) or mutant (MT) miR-13474 binding sites, were synthesized and strategically integrated into the pGL3 vector downstream of the firefly luciferase gene, thereby generating constructs denominated as ADAM17-WT and ADAM17-MT. Human 293 T cells (at a density of 5×10^4 cells per well) were seeded onto 24-well culture plates and subjected to co-transfection protocols employing miR-13474 mimics or a negative control (NC) miRNA mimic, in conjunction with control reporter plasmids pGL3, ADAM17-WT, or ADAM17-MT, facilitated by Lipofectamine 2000 as the transfection reagent. Post-transfection luciferase activities were assayed at the 24-h mark utilizing the Dual Luciferase Reporter Gene Assay System (Promega, USA), with firefly luciferase activity normalized against Renilla luciferase activity, in accordance with the manufacturer's specifications.

Exosomes loading of miR-13474 mimics

Sonication techniques were employed to facilitate the encapsulation of miR-13474 mimics within MSC-EVs. A mixture comprising MSC-EVs and 50 nM miR-13474 mimic or a negative control mimic was subjected to sonication under the parameters of 500 V, 2 kHz, 10% amplitude, employing a 4-s pulse followed by a 2-s pause for a total of six cycles. This procedure was executed using a Qsonica Sonicator Q700 (Misonix, USA), interspersed with a 2-min cooling period on ice. Subsequently, rna from EVs was subsequently extracted using the MiRNeasy micro kit (Qiagen, Germany). MiRNA were converted to cDNA using the MicroRNA Reverse Transcription Kit (Qiagen, Germany). Through the qRT—PCR (Vazyme, nanjing, China) determination of miR—13474 levels. The EVs overexpressing miR-13474 were called miR-13474^{mimic}-MSC-EVs and the negative control of miR-13474 mimics was called miR-13474$^{mimic\ NC}$-MSC-EVs. These miR-13474^{mimic}-MSC-EVs or miR-13474$^{mimic\ NC}$-MSC-EVs were cryopreserved at − 70 °C for subsequent experimental endeavors.

miR-13474 knockdown of exosomes

The negative control inhibitor, along with a 100 nM concentration of the miR-13474 inhibitor, was transiently transfected into MSCs at 70–80% confluency utilizing Lipofectamine 2000 as a transfection agent, within an Opti-MEM™ medium milieu (Invitrogen, USA). This procedure was conducted in 6-well culture plates. A temporal window of 4–6 h post-transfection served as the timepoint for substituting the existing culture medium with a FBS-devoid formulation, which was maintained for an ensuing 48-h period. Total RNA harvested from these inhibitor-transfected MSCs was earmarked for subsequent quantification of miR-13474. Extracellular vesicles emanating from miR-13474 inhibitor-transfected MSCs or their negative control inhibitor-transfected counterparts were isolated, purified, and washed in accordance with a previously established methodology. Subsequently, rna from EVs was subsequently extracted using the MiRNeasy micro kit (Qiagen, Germany). MiRNA were converted to cDNA using the MicroRNA Reverse Transcription Kit (Qiagen, Germany). Through the qRT—PCR (Vazyme, nanjing, China) determination of miR—13474 levels. The EVs knockdown miR-13474 were called miR-13474^{inhibitor}-MSC-EVs and the negative control of miR-13474 inhibitor was called miR-13474$^{inhibitor\ NC}$-MSC-EVs. These miR-13474^{inhibitor}-MSC-EVs or miR-13474$^{inhibitor\ NC}$-MSC-EVs were cryopreserved at − 70 °C for subsequent experimental endeavors.

Statistical analysis

Data were subjected to statistical scrutiny utilizing the GraphPad Prism 5 software suite (GraphPad, USA). All numerical values are articulated as the mean ± SEM. For bivariate analyses, an unpaired Student's t-test was deployed, while multivariate comparisons were executed employing one-way analysis of variance (ANOVA) Tukey's test. A p-value less than 0.05 was deemed to represent statistical significance.

Ethics approval and consent to participate

The study was approved by the Ethics Committee for Experimental Animals of Jiangsu University (Approval number: 2020280). All participants provided written informed consent prior to research participation. All experiments were performed in accordance with relevant named guidelines and regulations. All authors complied with the ARRIVE guidelines.

Data availability

All data needed to evaluate the conclusions in the paper are present in the paper and/or the Supplementary Materials. Additional data related to this paper may be requested from the authors.

Received: 23 April 2024; Accepted: 10 July 2024
Published online: 31 July 2024

References

1. Ji, C. *et al.* Engineered extracellular vesicle-encapsulated CHIP as novel nanotherapeutics for treatment of renal fibrosis. *NPJ Regen. Med.* **9**, 3. https://doi.org/10.1038/s41536-024-00348-0 (2024).
2. Chung, K. W. *et al.* Mitochondrial damage and activation of the STING pathway lead to renal inflammation and fibrosis. *Cell Metab.* **30**, 784-799.e785. https://doi.org/10.1016/j.cmet.2019.08.003 (2019).
3. Luyckx, V. A., Cherney, D. Z. I. & Bello, A. K. Preventing CKD in developed countries. *Kidney Int. Rep.* **5**, 263–277. https://doi.org/10.1016/j.ekir.2019.12.003 (2020).
4. Zhou, Z., Shi, L., Chen, B. & Qian, H. Regulation of regulated cell death by extracellular vesicles in acute kidney injury and chronic kidney disease. *Cytokine Growth Factor Rev.* https://doi.org/10.1016/j.cytogfr.2023.12.006 (2023).
5. Ji, C. *et al.* Exosomes derived from hucMSC attenuate renal fibrosis through CK1δ/β-TRCP-mediated YAP degradation. *Cell Death Dis.* **11**, 327. https://doi.org/10.1038/s41419-020-2510-4 (2020).
6. Ma, T. T. & Meng, X. M. TGF-β/Smad and renal fibrosis. *Adv. Exp. Med. Biol.* **1165**, 347–364. https://doi.org/10.1007/978-981-13-8871-2_16 (2019).
7. Humphreys, B. D. Mechanisms of renal fibrosis. *Annu. Rev. Physiol.* **80**, 309–326. https://doi.org/10.1146/annurev-physiol-022516-034227 (2018).
8. Chen, W. *et al.* Blocking interleukin-6 trans-signaling protects against renal fibrosis by suppressing STAT3 activation. *Theranostics* **9**, 3980–3991. https://doi.org/10.7150/thno.32352 (2019).
9. Salem, E. S., Grobe, N. & Elased, K. M. Insulin treatment attenuates renal ADAM17 and ACE2 shedding in diabetic Akita mice. *Am. J. Physiol. Renal. Physiol.* **306**, F629-639. https://doi.org/10.1152/ajprenal.00516.2013 (2014).
10. Palau, V. *et al.* Both specific endothelial and proximal tubular Adam17 deletion protect against diabetic nephropathy. *Int. J. Mol. Sci.* https://doi.org/10.3390/ijms22115520 (2021).
11. Cheng, J. *et al.* ADAM17 knockdown mitigates while ADAM17 overexpression aggravates cardiac fibrosis and dysfunction via regulating ACE2 shedding and myofibroblast transformation. *Front. Pharmacol.* **13**, 997916. https://doi.org/10.3389/fphar.2022.997916 (2022).
12. Guan, C. *et al.* The downregulation of ADAM17 exerts protective effects against cardiac fibrosis by regulating endoplasmic reticulum stress and mitophagy. *Oxid. Med. Cell Longev.* **2021**, 5572088. https://doi.org/10.1155/2021/5572088 (2021).
13. Xunian, Z. & Kalluri, R. Biology and therapeutic potential of mesenchymal stem cell-derived exosomes. *Cancer Sci.* **111**, 3100–3110. https://doi.org/10.1111/cas.14563 (2020).
14. El Agha, E. *et al.* Mesenchymal stem cells in fibrotic disease. *Cell Stem Cell* **21**, 166–177. https://doi.org/10.1016/j.stem.2017.07.011 (2017).
15. Matsuzaka, Y. & Yashiro, R. Therapeutic strategy of mesenchymal-stem-cell-derived extracellular vesicles as regenerative medicine. *Int. J. Mol. Sci.* https://doi.org/10.3390/ijms23126480 (2022).
16. Sun, Y. *et al.* Mesenchymal stem cells-derived exosomes for drug delivery. *Stem Cell Res. Ther.* **12**, 561. https://doi.org/10.1186/s13287-021-02629-7 (2021).
17. Tsiapalis, D. & O'Driscoll, L. Mesenchymal stem cell derived extracellular vesicles for tissue engineering and regenerative medicine applications. *Cells.* https://doi.org/10.3390/cells9040991 (2020).
18. Li, Q. *et al.* Requirements for human mesenchymal stem cell-derived small extracellular vesicles. *Interdiscip. Med.* https://doi.org/10.1002/inmd.20220015 (2023).
19. Aghajani Nargesi, A., Lerman, L. O. & Eirin, A. Mesenchymal stem cell-derived extracellular vesicles for kidney repair: current status and looming challenges. *Stem Cell Res. Ther.* **8**, 273. https://doi.org/10.1186/s13287-017-0727-7 (2017).
20. Birtwistle, L., Chen, X. M. & Pollock, C. Mesenchymal stem cell-derived extracellular vesicles to the rescue of renal injury. *Int. J. Mol. Sci.* https://doi.org/10.3390/ijms22126596 (2021).
21. Xiao, Z. *et al.* The Notch γ-secretase inhibitor ameliorates kidney fibrosis via inhibition of TGF-β/Smad2/3 signaling pathway activation. *Int. J. Biochem. Cell Biol.* **55**, 65–71. https://doi.org/10.1016/j.biocel.2014.08.009 (2014).
22. González-Foruria, I. *et al.* Dysregulation of the ADAM17/Notch signalling pathways in endometriosis: From oxidative stress to fibrosis. *Mol. Hum. Reprod.* **23**, 488–499. https://doi.org/10.1093/molehr/gax028 (2017).
23. Nastase, M. V., Zeng-Brouwers, J., Wygrecka, M. & Schaefer, L. Targeting renal fibrosis: Mechanisms and drug delivery systems. *Adv. Drug Deliv. Rev.* **129**, 295–307. https://doi.org/10.1016/j.addr.2017.12.019 (2018).
24. Xue, F. *et al.* Cardiomyocyte-specific knockout of ADAM17 ameliorates left ventricular remodeling and function in diabetic cardiomyopathy of mice. *Signal Transduct. Target Ther.* **7**, 259. https://doi.org/10.1038/s41392-022-01054-3 (2022).
25. Kefaloyianni, E. *et al.* ADAM17 substrate release in proximal tubule drives kidney fibrosis. *JCI Insight.* https://doi.org/10.1172/jci.insight.87023 (2016).
26. Genz, B. *et al.* Overexpression of miRNA-25-3p inhibits Notch1 signaling and TGF-β-induced collagen expression in hepatic stellate cells. *Sci. Rep.* **9**, 8541. https://doi.org/10.1038/s41598-019-44865-1 (2019).
27. Krampera, M. & Le Blanc, K. Mesenchymal stromal cells: Putative microenvironmental modulators become cell therapy. *Cell Stem Cell* **28**, 1708–1725. https://doi.org/10.1016/j.stem.2021.09.006 (2021).
28. Xie, Q. *et al.* What is the impact of human umbilical cord mesenchymal stem cell transplantation on clinical treatment?. *Stem Cell Res. Ther.* **11**, 519. https://doi.org/10.1186/s13287-020-02011-z (2020).
29. Grange, C., Skovronova, R., Marabese, F. & Bussolati, B. Stem cell-derived extracellular vesicles and kidney regeneration. *Cells.* https://doi.org/10.3390/cells8101240 (2019).
30. Cao, J. Y. *et al.* Exosomal miR-125b-5p deriving from mesenchymal stem cells promotes tubular repair by suppression of p53 in ischemic acute kidney injury. *Theranostics* **11**, 5248–5266. https://doi.org/10.7150/thno.54550 (2021).
31. Wang, Y. *et al.* Protective effect of miRNA-containing extracellular vesicles derived from mesenchymal stromal cells of old rats on renal function in chronic kidney disease. *Stem Cell Res. Ther.* **11**, 274. https://doi.org/10.1186/s13287-020-01792-7 (2020).
32. Liang, M., Zhang, D., Zheng, D., He, W. & Jin, J. Exosomes from miR-374a-5p-modified mesenchymal stem cells inhibit the progression of renal fibrosis by regulating MAPK6/MK5/YAP axis. *Bioengineered* **13**, 4517–4527. https://doi.org/10.1080/21655979.2022.2033465 (2022).
33. Xu, S. *et al.* Bone marrow mesenchymal stem cell-derived exosomal miR-21a-5p alleviates renal fibrosis by attenuating glycolysis by targeting PFKM. *Cell Death Dis.* **13**, 876. https://doi.org/10.1038/s41419-022-05305-7 (2022).

Acknowledgements

Linru Shi, Yuyan Hu, Houcheng Zeng contributed equally to this work. The authors thank the members of Qian lab for helpful discussion and paper preparation. This work was supported by the National Natural Science Foundation of China [Grant number 82172102], the Jiangsu Province's Major Project in Research and Development [Grant number BE2021689], the Natural Science Foundation of Jiangsu Province [Grant number

BK20220527], China Postdoctoral Science Foundation [Grant number 2023M731376], Technology Development Project of Jiangsu University [Grant number 20230593], Zhenjiang Key Laboratory of High Technology Research on Exosomes Foundation and Transformation Application [Grant number ss2018003].

Author contributions

Linru Shi performed experimental design, tissue procurement, data generation performed pathological assessments, data analysis and interpretation, and manuscript preparation; Yuyan Hu and Houcheng Zeng performed experimental design, data generation and data analysis; Hui Shi, Wenrong Xu and Yaoxiang Sun performed tissue procurement, data generation, interpretation and intellectual contribution. Hong Chu and Cheng Ji provided intellectual contribution and critically appraised the manuscript; Hui Qian conceived the study, designed experiments, interpreted data and prepared the manuscript.

Competing interests

The authors declare no competing interests.

Additional information

Supplementary Information The online version contains supplementary material available at https://doi.org/10.1038/s41598-024-67339-5.

Correspondence and requests for materials should be addressed to H.C., C.J. or H.Q.